

# Analysis of Geometric Multi-Bounced Virtual Scattering Channel Model for Dense Urban Street Environments

Hao Jiang, Zaichen Zhang, *Senior Member, IEEE*, Jian Dang, and Liang Wu

**Abstract**—This paper presents a generalized visual scattering channel model for car-to-car (C2C) mobile radio environments, in which an asymmetric directional antenna is deployed at the mobile transmitter (MT). The signals received at the mobile receiver (MR) from the MT are assumed to experience multi-bounced propagation paths. More importantly, the proposed model first separate the multi-bounced propagation paths into odd- and even-numbered-bounced propagation conditions. General formulations of the marginal probability density functions (PDFs) of the angle-of-departure (AoD) at the transmitter and angle-of-arrival (AoA) at the receiver have been derived for the above two conditions, respectively. From the proposed model, we derive an expression for the Doppler frequency due to the relative motion between the MT and MR, which broadens the research of the proposed visual street scattering channel model. The results show that the proposed model can fit those of the previous scattering channel models and the measurement results for dense urban street environments very well, which validate the generalization of the proposed virtual street channel model.

**Index Terms**—Visual scattering channel model, Car-to-Car, Dense urban street environments, Angle of departure, Angle of arrival, Doppler frequency.

## I. INTRODUCTION

With the rapid development of mobile Internet and the Internet of things (IoT), there are still some challenges that cannot be accommodated by the fourth generation (4G) wireless communication networks, such as the spectrum crisis and high energy consumption [1]. Therefore, research on the fifth generation (5G) wireless communication networks has been started, which has attracted great attention around the world. Compared to 4G, 5G networks are supposed to provide greatly enhanced capacity, spectral efficiency, energy efficiency, cost efficiency, mobility, data rate, connection density, etc., with a much reduced end-to-end latency [2]. To meet the 5G requirements, it is necessary to design the radio propagation channel model for mobile and wireless systems, especially for car-to-car (C2C) mobile radio environments [3], which has been regarded as one of the main research trends in next generation of mobile communication technology. Furthermore, the spatial characteristics of the multi-path channel are proven to be useful for high-performance multiple-input and multiple-output (MIMO) antenna systems. To efficiently create these

systems, it is essential to have a reliable understanding of the radio propagation characteristics of the transmission path between the transmitter and receiver, which leads to the design of effective signal processing techniques.

Geometrical modeling of the propagation channel has always been attractive for researchers, due to its many advantages [4]. The spatial characteristics of the multi-path channel, such as the probability density functions (PDFs) of the angle of departure (AoD) and angle of arrival (AoA) of the signals, can be utilized to analyze the performance of the MIMO and massive MIMO antenna systems. Therefore, a number of fundamental geometry-based statistical channel models have been proposed in the literature. References [5-9] focused on two-dimensional (2D) scattering channel models. For example, circular scattering models, ellipse scattering models [5], and asymmetric scattering models [9], which indicate that propagation takes place within the plane joining the tips of the transmitting and receiving antennas. Subsequently, many researchers have observed an angular spreading of the waves in the elevation plane because of the interaction of the waves with street buildings, ground, and other vertically disposed objects [10-13]. In 2010, Nawaz [10] presented a three-dimensional (3D) scattering model for macrocell environments, with a base station (BS) employing a directional antenna located outside the hemispheroid. Furthermore, Jiang [11] derived a generalized 3D scattering channel model for microcell environments, in which the scatterers are assumed to be located around the BS with a uniform distribution. Recently, a 3D ellipsoidal model for the mobile-to-mobile (M2M) radio propagation environments was proposed, in which the most frequent occurrence of the AoA of the received multi-path waves is located around the relative direction at each mobile station (MS) [12].

In general, the geometric scattering channel models above only focus on single-bounce, while multi-bounced propagation paths are not taken into account. In particular, for the dense urban street environments, the single-bounced assumption is rather restrictive because the street width is not sufficient to match the maximum of the elliptical scattering region. Therefore, there is a strong need for a generalized scattering channel model, which can be used to describe multi-bounced propagation paths. To overcome this problem and obtain the analytical solution, the concept of effective street width was presented in [14]. Subsequently, Ref. [15] provided a pseudo-geometrical scattering channel model, which visualized the double- and tri-bounced paths as single-bounce. Ghoraish [16]

This work is supported by NSFC projects (61571105, 61501109, and 61223001), 863 project (No. 2013AA013601), and Jiangsu NSF project (No. BK20140646).

The authors are with the National Mobile Communications Research Laboratory, Southeast University, Nanjing 210096, China.

Corresponding E-mail: jianghao@seu.edu.cn; zczhang@seu.edu.cn

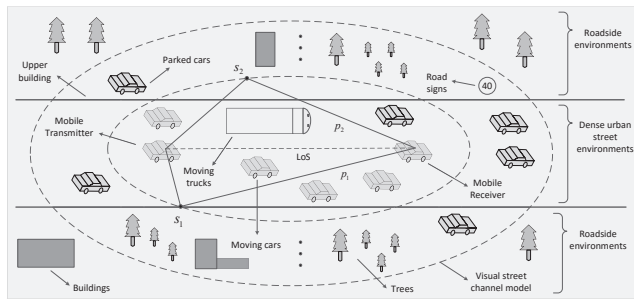


Fig. 1. Illustration of a typical C2C mobile radio environment and its corresponding visual scattering channel model for dense urban street environments.

presented the polar directional analysis of the urban non-line-of-sight (NLoS) propagation channel at 2.2 GHz, which is based on the measured data in Tokyo and Yokohama. The authors in [17] presented a reference model for a wideband MIMO channel based on the geometric elliptical scattering model. However, in [17], the mobile properties between the transmitter and receiver were not discussed in detail, and they are still restricted to the single-bounced propagation paths. In [18], a geometric street scattering channel model under line-of-sight (LoS) and NLoS propagation conditions for the outdoor communication environments was proposed, but they ignored multi-bounced propagation paths. MacCartney [19] conducted two measurement campaigns in urban microcellular environments, and path loss models suitable for the development of 5G standards were presented. Wang [20-21] later provided a vehicle-to-vehicle (V2V) channel model, which combines a two-ring model and a multiple confocal ellipses model, consisting of LoS, single-, and double-bounced waves. Rasekh [22] considered a street canyon approximation model, for the 60 GHz wireless channel in an urban environment, with rough surfaces. The authors in [23] proposed an adaptive geometry based on stochastic model for non-isotropic M2M communication environments, but they only focused on the single- and double-bounced conditions, and the condition of the multi-bounce has not been discussed in detail. However, when the signal endures unlimited-bounced propagation paths (i.e., the bounce number tends to be infinity), the previous scattering channel models are no longer applicable. Furthermore, the results and discussions above are restricted to the perspective of time domain, and the influence of the relative motion between the MSs on the distribution of the Doppler frequency, for the C2C mobile radio environments, has not been instigated in the previous literature.

In this paper, a generalized virtual scattering channel model for the microcell C2C street environments is proposed, in which multi-scatterings are taken into account and we visualize them as single-bounce scattering, as illustrated in Fig. 1. In this work, we first derive the closed-form expression for the marginal PDFs of the AoD and AoA for the odd- and even-numbered-bounced propagation paths. We then proceed to describe the Doppler shift due to the relative motion between the mobile transmitter (MT) and mobile receiver (MR). From numerical results and observations, the main advantages of this

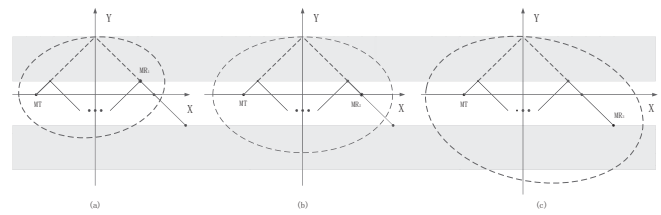


Fig. 2. The proposed visual street channel model for different positions of the MRs. (a) The receiver is located at the MR<sub>1</sub>. (b) The receiver is located at the MR<sub>2</sub>. (c) The receiver is located at the MR<sub>3</sub>.

paper are given as follows: (1) the proposed visual scattering channel model can be used to simulate the dense urban street environments, (2) it is possible to deduce single-, double-, triple-, and other multi-bounced paths of the street channel model, from our proposed visual scattering channel model. To the best of the authors' knowledge, this work has not been investigated before, (3) the effect of the asymmetric directional antenna employed at the MT in street environments is investigated, which analyzes more realistic positions of the MRs, (4) the total Doppler frequency due to the relative motion between the MT and MR is first taken into analysis in the proposed visual channel model, which broadens the research from the perspective of the frequency domain. Furthermore, the results are compared with those of the previous scattering channel models and measurement results, to validate the generalization of the proposed model. Accordingly, our proposed visual street channel model may be used to analyze the performance of M2M and IoT related to 5G wireless communication networks [2,24].

The rest of this paper is organized as follows: Section 2 discusses the proposed visual street channel model in detail. The spatial statistics of the proposed model are shown in Section 3. Based on the marginal PDFs of the AoD and AoA statistics, the total Doppler spectrum is investigated in Section 4. In Section 5, numerical results and discussions are given. Conclusions are finally drawn in Section 6.

## II. GENERALIZED VISUAL STREET CHANNEL MODEL

### A. Virtual model description

In order to sufficiently analyze and design the proposed visual street channel model, here we mainly concentrate on two important channel properties: scattering power distribution and Doppler power spectral density. In the proposed model, the scatterer density tapers off with the distance from the transmitter and receiver. Therefore, we adopt the scatterer non-uniform distribution came from the experimental measurements in [15] to describe the proposed mobile radio environments. On the other hand, the Doppler frequency distribution of the proposed street channel vary significantly with different moving properties in C2C mobile radio environments [24]. Furthermore, the Doppler distribution for the C2C channels is significantly different from the conventional Clarke distribution for scattering channels. To make the proposed street channel model more systematic, and in correspondence with the dense urban street environments, several common assumptions, as shown

in [10,11], are used to design the proposed visual channel model. They are as follows: (1) either the MT or the MR is surrounded by non-uniformly distributed scatterers confined with a visual elliptical channel model, (2) the channel model is two dimensional, which means that the MT, the MR, and the scatterers are all within the same plane, (3) all the scatterers have uniform random phases and the same scattering coefficient, (4) each scatterer is an omnidirectional reradiating element, independent of other scatterers.

The schematic of the multi-bounced propagation paths and its corresponding geometric elliptical scattering channel model are depicted in Fig. 1. In general, the transmission signal from the MT to the MR under multi-bounced propagation paths. However, for the conventional scattering channel models in [5-13], they almost concentrated on the single- and double-bounced models. For this we should propose multi-bounced scattering channel model, which can be utilized to accurately describe mobile radio communication environments. However, it is difficult to analyze multi-bounced propagation links in the proposed street channel model, here we can visualize them as single-bounced scattering scenarios. It can be observed that the scattering point  $s_2$  is identified in the roadside environments, and path  $p_2$  might be multi-scatterings. Obviously the visual scattering point for path  $p_2$  is identified in  $s_2$  which located on the cross point of the ellipse, note that the geometric path length of  $p_2$  is equal to that of  $p_1$ . Also, we assume that both the visual path  $p_2$  and the multi-bounced path  $p_1$  take equal path losses. Furthermore, we can observe that the reflected number of the signal is related to the angle at the MT, which is represented as  $\varphi = \arctan(2nW/D)$ , where  $D$  denotes the distance between the MT and MR, and  $W$  is street width. When the reflected number  $n$  is an odd number, then the signal will endure odd numbered-bounced propagation paths. Similarly, the signal will endure even-numbered-bounced propagation paths when  $n$  is an even number. Additionally, for the dense urban street environments, the propagation paths are not so long since the small distance between the MT and MR, which means that the channel always endures multi-scatterings. Therefore, the dominant loss in the channel is the scattering loss.

Figure 2 illustrates the proposed visual street channel model for different positions of the MRs and their corresponding visual single-bounced scattering channel models. It can be observed that the visual elliptical model is gradually skewed from the left to right when the receiver moves from the MR<sub>1</sub> to MR<sub>3</sub>. From this we should consider the rotation of the elliptical channel model. Let us define  $\theta$  as the tilt angle of the elliptical model. Moreover, the major and minor dimensions of the proposed visual scattering channel model are defined as  $a$  and  $b$  correspondingly, here we assume  $b \leq a$ . For this rotatable ellipse, the generalized equation can be expressed as [10]

$$\frac{(x \cos \theta + y \sin \theta)^2}{a^2} + \frac{(-x \cos \theta + y \sin \theta)^2}{b^2} = 1 \quad (1)$$

From Fig. 2 we can note that as the MR moves on the connection between the MR<sub>1</sub> and MR<sub>3</sub>, the proposed visual street channel model corresponds to different multi-bounced

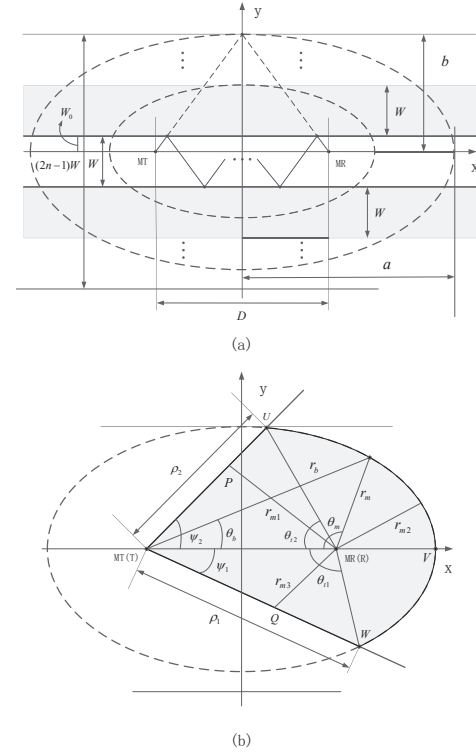


Fig. 3. The schematic of the odd-numbered-bounced propagation paths and its corresponding visual single-bounced geometric scattering channel model. (a) The geometrical description of the odd-numbered-bounced paths. (b) Geometric angles and path lengths of the proposed model for the odd-numbered-bounced conditions.

propagation conditions, including even- and odd-numbered-bounced paths. It is clearly observed that when the receiver is located at the MR<sub>1</sub>, the proposed visual elliptical channel model can be utilized to describe even-numbered-bounced propagation paths, as illustrated in Fig. 4. However, the proposed model presented the odd-numbered-bounced propagation paths as the receiver is identified at the other positions on the connection between the MR<sub>1</sub> and MR<sub>3</sub>. Based on the aforementioned analysis, it is necessary to separate the multi-bounced propagation paths into odd- and even-numbered-bounced propagation conditions, which will be analyzed in detail in the following subsections.

### B. Odd-numbered-bounced propagation paths

Figure 3 illustrates the proposed visual street channel model for the odd-numbered-bounced propagation paths. For simplicity, the model assumes that the receiver is located at the MR<sub>2</sub>, i.e.,  $\theta = 0$ , and its connection with the MT parallels the street walls for all odd-numbered-bounced propagation conditions. Therefore, let the connection of the MT and MR be  $x$ -axis, as shown in Fig. 3. Note that the focal length of the proposed visual elliptical channel model is larger than the distance between the MT and MR, and the focus are both assumed located on the  $x$ -axis. The multi-path azimuth departure angle at the MT is denoted by  $\theta_b$ , and the distance of the scattering object from the MT is defined as  $r_b$ . In order

to take more realistic positions of the MRs into account, the visual channel model assumes that an asymmetric directional antenna is deployed at the MT, spanning the azimuth range of  $[-\psi_1, \psi_2]$ . The same assumption is made in [9]. Therefore, the generalized equation of the visual channel model for odd-numbered-bounced propagation paths can be expressed as [10]

$$\frac{D^2 - 4Dr_b \cos \theta_b + 4r_b^2 \cos^2 \theta_b}{4a^2} + \frac{r_b^2 \sin^2 \theta_b}{b^2} = 1 \quad (2)$$

In this case, the major and minor dimensions of the visual elliptical channel model can be expressed as

$$a = (W_0 + (n-1)W) \csc \varphi \quad (3)$$

$$b = (n-1)W + W_0 \quad (4)$$

$$\text{and } 2c = 2(W_0 + (n-1)W) \cot \varphi, \quad n = 1, 2, 3, \dots \quad (5)$$

In Eqs. (3)-(5),  $W_0$  denotes the distance of the upper building to the MT, and  $2c$  is the focal length of the visual elliptical channel model, as illustrated in Fig. 3. By inserting (3)-(4) into (2), the standard equation of the proposed visual street channel model for odd-numbered-bounced paths can be obtained. Further, the distances from the visual boundary of the elliptical scattering channel model to the MT and MR are denoted by  $r_b$  and  $r_m$ , respectively. They are derived as functions of the angles measured at the MT and written as

$$r_b(\theta_b) = \frac{1}{2b^2 \cos^2 \theta_b + 2a^2 \sin^2 \theta_b} \times \left\{ Db^2 \cos \theta_b + \sqrt{D^2 b^4 \cos^2 \theta_b - (b^2 \cos^2 \theta_b + a^2 \sin^2 \theta_b)(D^2 b^2 - 4a^2 b^2)} \right\} \quad (6)$$

$$\text{and } r_m(\theta_b) = \sqrt{D^2 + r_b^2 - 2Dr_b \cos \theta_b}, \quad -\psi_1 \leq \theta_b \leq \psi_2 \quad (7)$$

Based on the proposed visual street model in Fig. 3, the lengths of the boundary of the scattering region, illustrated by the beam from the asymmetric directional antenna at the MT, are given by

$$\begin{aligned} \rho_1 &= r_b(\theta_b) \Big|_{\theta_b=\psi_1} \\ &= \frac{1}{2b^2 \cos^2(\psi_1) + 2a^2 \sin^2(\psi_1)} \times \left\{ Db^2 \cos(\psi_1) + \sqrt{D^2 b^4 \cos^2 \psi_1 - (b^2 \cos^2 \psi_1 + a^2 \sin^2 \psi_1)(D^2 b^2 - 4a^2 b^2)} \right\} \end{aligned} \quad (8)$$

$$\begin{aligned} \rho_2 &= r_b(\theta_b) \Big|_{\theta_b=\psi_2} \\ &= \frac{1}{2b^2 \cos^2(\psi_2) + 2a^2 \sin^2(\psi_2)} \times \left\{ Db^2 \cos(\psi_2) + \sqrt{D^2 b^4 \cos^2 \psi_2 - (b^2 \cos^2 \psi_2 + a^2 \sin^2 \psi_2)(D^2 b^2 - 4a^2 b^2)} \right\} \end{aligned} \quad (9)$$

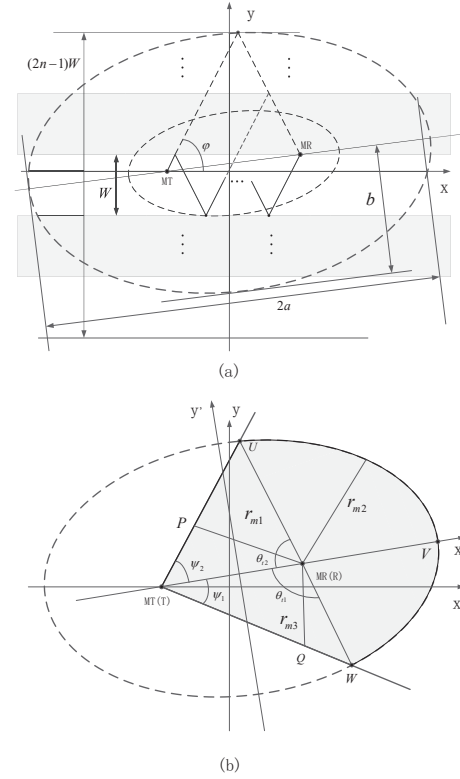


Fig. 4. The schematic of the even-numbered-bounced propagation paths and its corresponding visual single-bounced geometric scattering channel model. (a) The geometrical description of the even-numbered-bounced paths. (b) Geometric angles and path lengths of the proposed model for the even-numbered-bounced conditions.

### C. Even-numbered-bounced propagation paths

The proposed visual street channel model for the even-numbered-bounced paths is shown in Fig. 4. Note that defining the connection of the MT and MR as the  $x$ -axis of the visual elliptical model is quite unreasonable [15]. Let us assume that the major dimension of the visual elliptical channel model is located on the  $x'$ -axis. While it is difficult to obtain the generalized equation of the visual scattering channel model directly from the rectangular coordinate  $(x, y)$  since the number of the paths and the number of reflections are not equal. By transforming  $(x, y)$  into  $(x', y')$ , the generalized equation can be derived as

$$\frac{(x')^2}{a^2} + \frac{(y')^2}{b^2} = 1 \quad (10)$$

$$\begin{aligned} \frac{(2x - W_0 \cot \varphi_0)^2 (\cos \varphi_0 - \sin \varphi_0)^2}{4a^2} + \frac{(2y - W_0)^2 (\cos \varphi_0 + \sin \varphi_0)^2}{4b^2} = 1 \end{aligned} \quad (11)$$

In Eq. (11), the transformation angle from the rectangular coordinate  $(x, y)$  to  $(x', y')$  is given by

$$\varphi_0 = \arctan \left\{ \frac{W_0}{D - W_0 \cot \varphi} \right\} \quad (12)$$

Similar as before, the major and minor dimensions of the visual elliptical channel model for even-numbered-bounced paths can be expressed as

$$a = (2nW - W_0) \csc \varphi \quad (13)$$

$$b = nW - W_0 \quad (14)$$

$$\text{and } c = (2nW - W_0) \cot \varphi, \quad n = 1, 2, 3, \dots \quad (15)$$

As described before, substituting (13)-(14) into (11), the standard equation of the visual street channel model for even-numbered-bounced paths can be obtained.

### III. SPATIAL CHARACTERISTICS OF THE STREET CHANNEL MODEL

In wireless environments, the spatial characteristics that describe the AoD and AoA statistics of the multi-bounced components are quite useful. This can be used in the performance evaluation of wireless communication systems employing MIMO antenna arrays, and broaden the research from the perspective of frequency domain. We begin this section with a discussion of the scattering distribution for dense urban street environments, which is measured in [15]. We then analyze the marginal PDFs of the AoD and AoA statistics, viewed at the MT and MR, respectively.

#### A. Scattering distribution

From the illustration of the C2C mobile radio environments in Fig. 1, it can be found that the scattering region gradually increases with an increase in the number of reflections. In general, the scatterer density tapers off with the distance from the transmitter and receiver. Therefore, it is necessary to present scatterer non-uniform distribution in the proposed C2C street channel model. However, we can observe if we perform experimental measurements for the proposed C2C dense urban street environments, the analysis will be very complex. Here, we adopt the experimental measurements in [15] of the scattering distribution to describe the proposed mobile radio environments. Furthermore, it is observed that the scattering distribution has an elliptical shape, but it is different from the conventional scatterer Gaussian and Exponential distributions in that most scatterers are distributed along the street. From this we can clearly describe the spatial characteristics of the proposed visual street channel model. Therefore, the scattering power distribution in [15] can be expressed as

$$p(x, y) = \exp \left\{ -\sqrt{A_x(x-c)^2 + A_y \cdot y^2} - \sqrt{A_x(x+c)^2 + A_y \cdot y^2 + C_{xy}} \right\} \quad (16)$$

where  $A_x$  and  $A_y$  are loss coefficients along  $x$  and  $y$  axes, respectively, and  $C_{xy}$  is a constant. After Jacobian of the

inverse transformation, the joint PDF of the AoD can be written as

$$p(r_b, \theta_b) = \frac{p(x, y)}{|J(x, y)|} \Bigg|_{\substack{x=r_b \cos \theta_b - D/2 \\ y=r_b \sin \theta_b}} \\ = r_b \exp \left\{ -\sqrt{A_x \left( r_b \cos \theta_b - \frac{D}{2} - c \right)^2 + r_b^2 A_y \sin^2 \theta_b} - \sqrt{A_x \left( r_b \cos \theta_b - \frac{D}{2} + c \right)^2 + r_b^2 A_y \sin^2 \theta_b + C_{xy}} \right\} \quad (17)$$

Similarly, at the MR, the joint PDF of the AoA can be given by

$$p(r_m, \theta_m) \\ = r_m \exp \left\{ -\sqrt{A_x \left( \frac{D}{2} - r_m \cos \theta_m - c \right)^2 + r_m^2 A_y \sin^2 \theta_m} - \sqrt{A_x \left( \frac{D}{2} - r_m \cos \theta_m + c \right)^2 + r_m^2 A_y \sin^2 \theta_m + C_{xy}} \right\} \quad (18)$$

In the following, we performed experimental measurements in [15] for three streets, with the different widths of 26m, 18m, and 10m. The distances of the MT and MR from the walls of the same side are set as 5m, 5m, and 3m, respectively. The MT to the MR distance is fixed at 60m, and the asymmetric directional antennas at the MT having main lobes of  $[-40^\circ, 80^\circ]$  and  $[-20^\circ, 40^\circ]$  are assumed. From the experimental measurements, for the dense urban areas [15], the loss coefficients ( $A_x, A_y$ ) for the above three cases are derived as  $(1.0 \times 10^{-4}, 1.0 \times 10^{-3})$ ,  $(2.0 \times 10^{-4}, 2.0 \times 10^{-3})$ , and  $(2.1 \times 10^{-4}, 3.0 \times 10^{-3})$ , respectively.

#### B. Marginal PDF of the AoD

Here, the marginal PDF of the AoD can be derived by integrating the joint PDF in (17) over the geometric path length  $r_b$ . Therefore, the AoD PDF is given by [6]

$$p(\theta_b) = \frac{1}{A} \int_0^{r_b(\theta_b)} p(r_b, \theta_b) dr_b \quad (19)$$

For the proposed visual street channel model, the total scattering region created by the directional antenna at the MT can be calculated as

$$A = \int_{-\psi_1}^{\psi_2} p(r_b, \theta_b) d\theta_b \\ = \int_{-\psi_1}^{\psi_2} r_b \exp \left\{ -\sqrt{A_x \left( r_b \cos \theta_b - \frac{D}{2} - c \right)^2 + r_b^2 A_y \sin^2 \theta_b} - \sqrt{A_x \left( r_b \cos \theta_b - \frac{D}{2} + c \right)^2 + r_b^2 A_y \sin^2 \theta_b + C_{xy}} \right\} d\theta_b \quad (20)$$

In previous sections,  $r_b(\theta_b)$  and  $A$  were given by (6) and (20), respectively. Substituting (6) and (20) into (19), the marginal PDF of the AoD can be obtained.

### C. Marginal PDF of the AoA

Similarly, at the MR, the marginal PDF of the AoA can be obtained within the proposed visual street channel model. Note that the arriving angles  $\theta_{t1}$  and  $\theta_{t2}$  (i.e.,  $\theta_{t1} \leq \theta_{t2}$ ) are calculated to separate the above scattering region into three partitions within the azimuth plane. Here the angle  $\theta_{t1}$  and  $\theta_{t2}$  are defined as azimuthal threshold angles, and can be written as the functions of the number of reflections and beam-width of the directional antenna. Therefore, the equations can be written in the closed form as

$$\theta_{t1} = \arctan \left\{ \frac{\rho_1 \sin(\psi_1)}{D - \rho_1 \cos(\psi_1)} \right\} \quad (21)$$

$$\theta_{t2} = \arctan \left\{ \frac{\rho_2 \sin(\psi_2)}{D - \rho_2 \cos(\psi_2)} \right\} \quad (22)$$

Owing to the directional antenna at the MT (i.e., MT'), clipping occurs in the scattering region. Note that the distances from the MR to the visual boundary of the street channel model are obviously different among these three parts, they are: the areas of *TRU* (i.e., *T'RU*), *UVWR*, and *TRW* (i.e., *T'RW*), respectively, as shown in Figs. 3 and 4. Therefore, the joint PDFs of the AoA in  $0 \leq \theta_m \leq 2\pi$  are shown as follows:

Case 1:  $0 \leq \theta_m \leq \theta_{t2}$

$$p_1(\theta_m) = \frac{1}{A} \int_0^{r_{m1}(\theta_m)} p(r_m, \theta_m) dr_m \quad (23)$$

It can be found in the scattering area of *TRU* (i.e., *T'RU*) from Figs. 3 and 4. Let the function  $r_{m1}(\theta_m)$  be the scatterers at the boundary of the line *MS-P*, which can be expressed as

$$r_{m1}(\theta_m) = D \sin(\psi_1) \csc(\psi_1 + \theta_m) \quad (24)$$

Substitute (20) into (23), the marginal PDF of the AoA for the Case 1 can be obtained by integrating the joint PDF of the AoA in (18) over the function in (24), as derived in [6].

Case 2:  $\theta_{t2} \leq \theta_m \leq 2\pi - \theta_{t1}$

$$p_2(\theta_m) = \frac{1}{A} \int_0^{r_{m2}(\theta_m)} p(r_m, \theta_m) dr_m \quad (25)$$

For the scattering area of *UVWR*, the function  $r_{m2}(\theta_m)$  denotes the distance of the MR from the scattering objects located at the visual boundary of the elliptical scattering region, which has been determined in (7), and can be further rewritten as

$$r_{m2}(\theta_m) = \frac{1}{2b^2 \cos^2 \theta_m + 2a^2 \sin^2 \theta_m} \times \left\{ D b^2 \cos \theta_m + \sqrt{D^2 b^4 \cos^2 \theta_m - (b^2 \cos^2 \theta_m + a^2 \sin^2 \theta_m)(D^2 b^2 - 4a^2 b^2)} \right\} \quad (26)$$

As in earlier derivations, the marginal PDF of the AoA statistics for the Case 2 can be obtained by integrating the joint PDF in (18) over the Eq. (26).

Case 3:  $2\pi - \theta_{t1} \leq \theta_m \leq 2\pi$

$$p_3(\theta_m) = \frac{1}{A} \int_0^{r_{m3}(\theta_m)} p(r_m, \theta_m) dr_m \quad (27)$$

In this part (i.e., the area of *TRW* or *T'RW*), we can define the function  $r_{m3}(\theta_m)$  as the scatterers at the boundary of the line *MS-Q*, which can be calculated as

$$r_{m3}(\theta_m) = D \sin(\psi_2) \csc(\psi_2 + \theta_m) \quad (28)$$

Like Case 1 and 2 above, substituting (20) into (27), the marginal AoA PDF for Case 3 can be obtained by integrating the joint AoA PDF in (18) over the path length  $r_{m3}(\theta_m)$  in (28).

## IV. DOPPLER FREQUENCIES

In the proposed visual street channel model, the received signal at the MR experiences spread in the frequency spectrum caused by the relative motion between the MT and MR. For readability purposes, we assume an omnidirectional antenna at the MR, then the relationship between the arriving angles (i.e.,  $\theta_b$  and  $\theta_m$ ) and the Doppler shift of a sinusoidal signal can be expressed as [13,16]

$$f_b = \frac{v_b}{c} f_{c1} \cos(\phi_{vb} - \theta_b) = f_{m1} \cos(\phi_{vb} - \theta_b) \quad (29)$$

$$f_m = \frac{v_m}{c} f_{c2} \cos(\phi_{vm} - \theta_m) = f_{m2} \cos(\phi_{vm} - \theta_m) \quad (30)$$

where  $v_b$  is the moving velocity of the MT,  $\phi_{vb}$  is the moving direction with respect to the direct LoS component,  $c$  is the velocity of light,  $f_{c1}$  and  $f_{c2}$  are the frequencies of the carrier signal and baseband signal, respectively. Similarly, at the MR,  $v_m$  is the relative moving velocity of the MR,  $\phi_{vm}$  denotes the angle between the direction of the MR with respect to the  $x$ -axis (i.e.,  $x'$ -axis). While  $f_b$  and  $f_m$  stand for the maximum Doppler frequencies for the MT and MR, respectively (i.e.,  $f_b \leq |f_{m1}|$  and  $f_m \leq |f_{m2}|$ ). Based on the marginal PDF of the AoD in (19), the PDF of the Doppler frequency at the MT can be obtained by [16]

$$p(f_b) = \frac{1}{f_{m1} \sqrt{1 - (f_b/f_{m1})^2}} \times \left\{ p(\phi_{vb} - \arccos(f_b/f_{m1})) + p(\phi_{vb} + \arccos(f_b/f_{m1})) \right\} f_{m1} \cdot \cos(\phi_{vb} - \psi_2) \leq f_b \leq f_{m1} \cdot \cos(\phi_{vb} + \psi_1) \quad (31)$$

Note that the MT and MR are both in motion. For simplicity, we introduce the concept of the relatively moving velocity, which indicates that the MT is relatively static, while the MR is in relative motion. Here we can define MR moving in an arbitrary direction  $\phi_v$  in the azimuth plane. Owing to the relative motion between the MT and MR, it has been shown that the PDF of the Doppler frequency is significantly related to the direction of relative motion. Moreover, on the basis of the marginal PDF of the AoA in (23), (25), and (27), when the MR moves towards the MT, i.e.,  $\phi_v = 0$ , the PDF of the

Doppler shift can be expressed as

$$p(f_m) = \begin{cases} \frac{1}{f_{m2} \cdot \sqrt{1 - (f_m/f_{m2})^2}} \times \left\{ p_3 \left( -\arccos(f_m/f_{m2}) \right) \right. \\ \quad \left. + p_1 \left( \arccos(f_m/f_{m2}) \right) \right\}, \\ \quad f_{m2} \cdot \cos(\theta_{t1}) \leq f_m \leq f_{m2} \\ \frac{1}{f_{m2} \cdot \sqrt{1 - (f_m/f_{m2})^2}} \times \left\{ p_2 \left( -\arccos(f_m/f_{m2}) \right) \right. \\ \quad \left. + p_1 \left( \arccos(f_m/f_{m2}) \right) \right\} \\ \quad f_{m2} \cdot \cos(\theta_{t2}) \leq f_m \leq f_{m2} \cdot \cos(\theta_{t1}) \\ \frac{1}{f_{m2} \cdot \sqrt{1 - (f_m/f_{m2})^2}} \times \left\{ p_2 \left( -\arccos(f_m/f_{m2}) \right) \right. \\ \quad \left. + p_2 \left( \arccos(f_m/f_{m2}) \right) \right\} \\ \quad -f_{m2} \leq f_m \leq f_{m2} \cdot \cos(\theta_{t2}) \end{cases} \quad (32)$$

On the other hand, when the receiver moves perpendicular to the line joining the MT and MR (i.e.,  $\phi_v = \pi/2$ ), the PDF of the Doppler frequency at the MR can be written as

$$p(f_m) = \begin{cases} \frac{1}{f_{m2} \cdot \sqrt{1 - (f_m/f_{m2})^2}} \times \left\{ p_1 \left( \pi/2 - \arccos(f_m/f_{m2}) \right) \right. \\ \quad \left. + p_3 \left( \pi/2 + \arccos(f_m/f_{m2}) \right) \right\} \\ \quad f_{m2} \sin(\theta_{t2}) \leq f_m \leq f_{m2} \\ \frac{1}{f_{m2} \cdot \sqrt{1 - (f_m/f_{m2})^2}} \times \left\{ p_2 \left( \pi/2 - \arccos(f_m/f_{m2}) \right) \right. \\ \quad \left. + p_3 \left( \pi/2 + \arccos(f_m/f_{m2}) \right) \right\} \\ \quad 0 \leq f_m \leq f_{m2} \cdot \sin(\theta_{t2}) \\ \frac{1}{f_{m2} \cdot \sqrt{1 - (f_m/f_{m2})^2}} \times \left\{ p_2 \left( \pi/2 - \arccos(f_m/f_{m2}) \right) \right. \\ \quad \left. + p_1 \left( \pi/2 + \arccos(f_m/f_{m2}) \right) \right\} \\ \quad -f_{m2} \sin(\theta_{t1}) \leq f_m \leq 0 \\ \frac{1}{f_{m2} \cdot \sqrt{1 - (f_m/f_{m2})^2}} \times \left\{ p_3 \left( \pi/2 - \arccos(f_m/f_{m2}) \right) \right. \\ \quad \left. + p_1 \left( \pi/2 + \arccos(f_m/f_{m2}) \right) \right\} \\ \quad -f_{m2} \leq f_m \leq -f_{m2} \cdot \sin(\theta_{t1}) \end{cases} \quad (33)$$

Next, the concept of the total Doppler frequency of the proposed visual street channel model is introduced, which is formed by the relative motion between the MT and MR. Moreover, the PDFs of the Doppler frequency at the MT and MR are assumed to be two independent random variables. To

obtain the PDF of the total Doppler frequency, the characteristic functions are taken into account, which can be defined as

$$p_b(\omega) = \int_{-\infty}^{\infty} p(f_b) e^{j\omega f_b} df_b \quad (34)$$

$$p_m(\omega) = \int_{-\infty}^{\infty} p(f_m) e^{j\omega f_m} df_m \quad (35)$$

By using (34) and (35), we can find the characteristic function  $p(\omega)$  of the total Doppler frequency by the product of two characteristic functions as

$$p(\omega) = p_b(\omega) \cdot p_m(\omega) \quad (36)$$

Consequently, by using the inversion Fourier transform formula for (36), the PDF can be derived as

$$p(f) = \frac{1}{2\pi} \int_{-\infty}^{\infty} p(\omega) e^{j\omega f} d\omega \quad (37)$$

Inserting (36) into (37), the PDF of the total Doppler frequency can be obtained. Further, we can analyze the proposed visual street model from the perspective of the frequency domain. Additionally, we can see if the AoA of the signal at the receiver is assumed to be uniform, the Doppler spectra is given by Clarke's model [8].

## V. NUMERICAL RESULTS AND DISCUSSIONS

To establish the validity and generalizability of the proposed visual street channel model, several comparisons are made between the proposed model and some notable models and measured data. The results illustrate that the distributions of the AoD/AoA statistics and the Doppler shift of the proposed visual street model fit the Ghorraishi model [15], the Avazov model [18], the Zhou model [6], and the measured data [26] very well.

### A. Distribution of the AoD and AoA PDFs

The marginal PDF of the AoD statistics corresponding to the beam-width of the directional antenna (i.e.,  $\psi_1$  and  $\psi_2$ ) and the street width (i.e.,  $W$ ), is shown in Fig. 5. Note that the values of the AoD PDF tend to be lower with decreasing the width of the streets. It also can be observed that the PDF of the AoD significantly decreases in  $0 \leq \theta_b \leq \psi_2$ , and similar behavior can be seen in  $-\psi_1 \leq \theta_b \leq 0$ , which agrees with the results in the Petrus model [7]. Meanwhile, the PDF of the submitted signals with smaller values of the AoD is relatively large. Furthermore, when the MT is equipped with the omnidirectional antenna, the distribution of the AoD PDF fits very well with the simulation results in [25], demonstrating that the results above are accurate and applicable to describe the street wireless environments.

The impacts of changing the beam-widths  $\psi_1$  and  $\psi_2$  on the PDFs of the AoA statistics are shown in Fig. 6. It can be found that the missing sections of curves enlarge slowly accompanied by an increase in beam-widths, resulting from the irregular scattering region. Furthermore, the curves of the PDFs are asymmetric and have two 'corners' located in the left

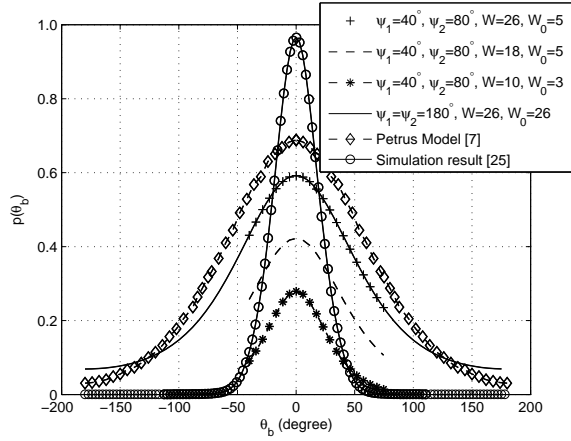


Fig. 5. Marginal PDF of the AoD in terms of the different beam-widths and street widths when  $D=60\text{m}$ .

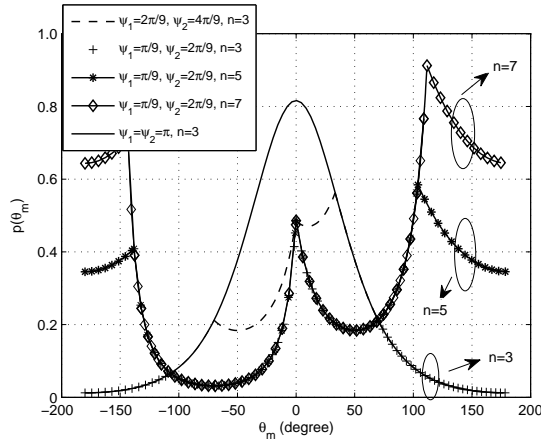


Fig. 6. Marginal PDF of the AoA in terms of the different beam-widths and the number of reflections when  $W=18\text{m}$ ,  $W_0=5\text{m}$ , and  $D=60\text{m}$ .

and right parts, which occur at the azimuth angle  $\theta_m = -\theta_{t1}$  and  $\theta_m = \theta_{t2}$ , respectively, only depending upon the visual asymmetric geometrical channel model, as seen in Figs. 3 and 4. With decreasing  $\psi_1 + \psi_2$  with less scatterers in the areas illuminated by the directional antenna, the AoA PDFs have lower values on both sides of the curves in  $-\theta_{t1} \leq \theta_m \leq \theta_{t2}$ , whereas the values at  $\phi_m = 0$  tend to be equal. The analysis above agrees with the results in [15], clearly demonstrating the MIMO and massive MIMO compact antenna systems as promising technologies for wireless street environments.

The effects of changing the width of the visual street and the number of reflections (i.e.,  $n$ ) of the received signal for the AoA PDFs are illustrated in Fig. 7. It is observed that the AoA statistics decrease first and increase to a local maximum value with higher AoAs, and then decreases gradually in  $\theta_{t2} \leq \theta_m \leq \pi$ , a similar behavior can be seen in  $-\pi \leq \theta_m \leq 0$ . Moreover, it is clear that when the street width is fixed (i.e.,  $W=60\text{m}$ ), the PDFs of the AoA tend to be equal for  $0 \leq \theta_m \leq \theta_{t2}$ . Further, the AoA statistics are increasing gradually with increasing the number of reflections when the values are in  $\theta_{t2} \leq \theta_m \leq \pi$ . Comparing the proposed

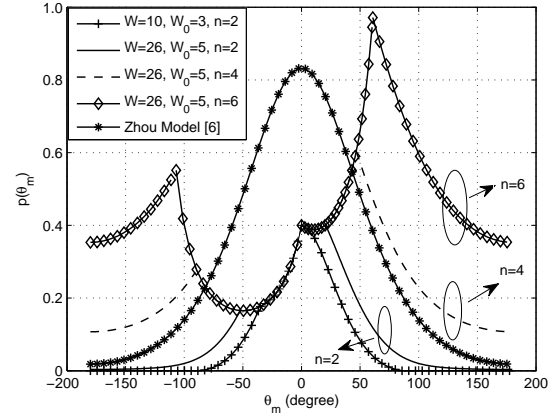


Fig. 7. Marginal PDF of the AoA in terms of the different street widths and the number of reflections when  $\psi_1 = 40^\circ$ ,  $\psi_2 = 80^\circ$ , and  $D=60\text{m}$ .

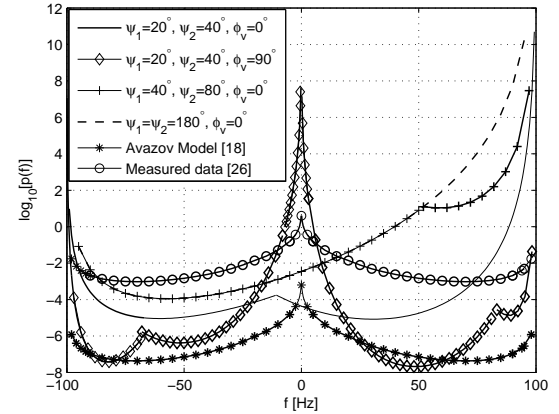


Fig. 8. Distribution of the total Doppler shift with respect to the different relative moving direction, the beam-width, and the number of reflections when  $D=60\text{m}$ ,  $W=26\text{m}$ ,  $W_0=5\text{m}$ ,  $f_{m1} = f_{m2}=100\text{Hz}$ ,  $A_x=1.0 \times 10^{-4}$ , and  $A_y=1.0 \times 10^{-3}$ .

visual street channel model with the Zhou Model [6], we can see that the distribution of the AoA PDFs has similar trends for the omnidirectional antenna (i.e.,  $\psi_1=\psi_2=180^\circ$ ) at the MT, irrespective of macrocell and microcell environments. From the numerical results and discussions above, we can draw a conclusion that the distributions of the odd- and even-numbered-bounced propagation paths would tend to be the same when the number of reflections of the received signal tends to infinity (i.e.,  $n \rightarrow \infty$ ).

### B. Distribution of the Doppler frequency

The distribution of the total Doppler shift versus the direction of relative motion of the MR (i.e.,  $\phi_v$ ) and the beam-widths of the directional antenna at the MT is shown in Fig. 8. It can be noted that when the MR moves towards the MT, the values of the Doppler shift significantly increase, accompanied by an increase in the beam-width  $\psi_1$  and  $\psi_2$ , which is due to the fact that a decrease in the beam-width could diminish the amount of scatterers and then reduce the multi-

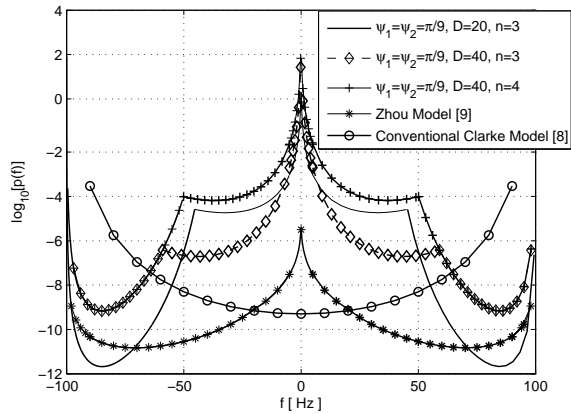


Fig. 9. Distribution of the total Doppler shift with respect to the distance between the MT and MR, and the number of reflections when  $\phi_v = \pi/2$ ,  $W=26\text{m}$ ,  $W_0=5\text{m}$ ,  $f_{m1} = f_{m2}=100\text{Hz}$ ,  $A_x=1.0 \times 10^{-4}$ , and  $A_y=1.0 \times 10^{-3}$ .

path components. On the other hand, for an omnidirectional antenna, the Doppler PDFs of the proposed visual street channel models are significantly different from the traditional U-shaped Doppler distribution [8, 18]. It also can be noted that the PDFs are skewed toward higher frequencies when the omnidirectional antenna is deployed at the MT, resulting from the unbalanced number of illuminated scattering objects with respect to the  $x$ -axis of motion of the MR. The analysis in Fig. 8 fits very well with the results in [26], demonstrating the accuracy of the total Doppler shift in the proposed model. Furthermore, the curves of the Doppler PDFs are asymmetric and have two 'corners' located in the left and right parts, which is in agreement with the discussion in Fig. 5. This clearly indicates that the Doppler frequency is significantly related to the distribution of power over the AoD and AoA statistics.

The influence of the distance between the MT and MR (i.e.,  $D$ ) and the number of reflections on the total Doppler distribution is shown in Fig. 9. When the receiver moves perpendicular to the direct LoS component, most of the spectral components remain near the central frequencies (i.e.,  $|f|=0$ ), an observation that is in agreement with the results reported in [9]. Meanwhile, the curves of all PDFs are asymmetric. This is because the clipped scattering region is geometrically asymmetric, as illustrated in Figs. 3 and 4, and the number of multi-path components corresponding to the positive and negative Doppler frequencies is unequal [12]. Moreover, it is observed that the PDFs of Doppler frequency gradually increase with an increase in the distance between the MT and MR or the number of reflections. Besides that, comparisons between the above theoretical discussions with the Wang model [20] show that the distribution trends are both in agreement with each other, which validate the generalization of the proposed virtual street channel model.

## VI. CONCLUSION

In this paper, a generalized visual scattering channel model for multi-bounced propagation paths in the dense urban street environments has been observed. The proposed model first

has the ability to describe the multi-reflecting propagation paths for odd- and even-numbered-bounced propagation paths. On the basis of the marginal PDFs of the AoD and AoA statistics, the distributions of the total Doppler frequency due to the relative motion between the MT and MR have been analyzed, which broaden the analysis of the visual street channel model from the perspective of the frequency domain. Furthermore, we have performed the spatial characteristics for different beam-widths, street widths, distance between the MT and MR, the number of reflection, and the relative moving direction. Comparisons between our theoretical results and several previous scattering channel models show that the proposed visual scattering channel model is accurate and applicable to depict dense urban street scenarios.

## VII. ACKNOWLEDGE

We thank Professor Jie Zhou, Department of Electronic and Electrical Engineering, Nanjing University of Information Science and Technology, for helping us complete this study successfully.

## REFERENCES

- [1] P.P. Tayade, V.M. Rohokale: 'Enhancement of Spectral Efficiency, Coverage and Channel Capacity for Wireless Communication Towards 5G', International Conf. on Pervasive Computing (ICPC), Pune, India, 8-10 Jan. 2015, pp. 1-5.
- [2] DOCOMO 5G White Paper: '5G Radio Access: Requirements, Concept and Technologies', NTT DOCOMO, INC. July 2014.
- [3] J. Karedal et al., 'A Geometry-Based Stochastic MIMO Model for Vehicle-to-Vehicle Communications', IEEE Trans. Wireless Commun., vol. 8, no. 7, pp. 3646-3657, Jul. 2009.
- [4] Y.F. Chen, V.K. Dubey: 'Accuracy of Geometric Channel-Modeling Methods', IEEE Trans. on Veh. Technol., vol. 53, no. 1, pp. 82-93, Jan. 2004.
- [5] R.B. Ertel, J.H. Reed: 'Angle and Time of Arrival Statistics for Circular and Elliptical Scattering Model', IEEE Journal on Selected Areas in Commun., vol. 17, no. 11, pp. 1829-1840, Nov. 1999.
- [6] J. Zhou, H. Jiang, H. Kikuchi: 'Geometry-based Statistical Channel Model and Performance for MIMO Antennas', Int. Journal of Commun. Systems, vol. 29, no. 3, pp. 459-477, 2016.
- [7] P. Petrus, T.S. Rappaport: 'Geometrical-Based Statistical Macrocell Channel Model for Mobile Environments', IEEE Trans. on Commun., vol. 50, no. 3, pp. 495-502, 2002.
- [8] L. Jiang, S.Y. Tan: 'Geometrically Based Statistical Channel Models for Outdoor and Indoor Propagation Environments', IEEE Trans. on Veh. Technol., vol. 56, no. 6, pp. 3587-3593, 2007.
- [9] J. Zhou, Z.G. Cao, H. Kikuchi: 'Asymmetric Geometrical-Based Statistical Channel Model and its Multiple-Input and Multiple-Output Capacity', IET Communications, vol. 8, no. 1, pp. 1-10, 2014.
- [10] S.J. Nawaz, B.H. Qureshi, N.M. Khan: 'A Generalized 3-D Scattering Model for a Macrocell Environment with a Directional Antenna at the BS', IEEE Trans. on Veh. Technol., vol. 59, no. 7, pp. 3193-3204, 2010.
- [11] H. Jiang, J. Zhou, H. Kikuchi: 'Angle and Time of Arrival Statistics for a 3-D Pie-Cellular-Cut Scattering Channel Model', Springer Wireless Pers. Commun., vol. 78, no. 2, pp. 851-865, 2014.
- [12] M. Riaz, N.M. Khan, S.J. Nawaz: 'A Generalized 3-D Scattering Channel Model for Spatiotemporal Statistics in Mobile-to-Mobile Communication Environment', IEEE Trans. on Veh. Technol., vol. 64, no. 10, pp. 4399-4410, Oct. 2015.
- [13] S.X. Qu: 'An Analysis of Probability Distribution of Doppler Shift in Three Dimensional Mobile Radio Environments', IEEE Trans. on Veh. Technol., vol. 58, no. 4, pp. 1634-1639, 2009.
- [14] M. Marques, M. Correia: 'A Wideband Directional Channel Model for UMTS Micro-cells', Processings of the IEEE International Symposium on Personal, Indoor and Mobile Radio Communications (PIMRC'01), San Diego, CA, Vol. 1, Sept. 2001, pp. B-122-B-126.

- [15] M. Ghoraiishi, J.I. Takada, T. Imai: 'A Pseudo-Geometrical Channel Model for Dense Urban Line-of-Sight Street Microcell', IEEE 17th International Symposium on Personal, Indoor and Mobile Radio Commun., Helsinki, Finland, 11-14 Sept. 2006, pp. 1-5.
- [16] M. Ghoraiish, G. Ching, N. Lertsirisopon: 'Polar Directional Characteristics of the Urban Mobile Propagation Channel at 2.2 GHz', 3rd European Conference on Antennas and Propagation, Berlin, Germany, 23-27 March 2009, pp. 892-896.
- [17] M. Patzold, B. O. Hogstad: 'A Wideband MIMO Channel Model Derived From the Geometrical Elliptical Scattering Model', International Symposium on Wireless Commun. and Mobile Computing, Valencia, Spain, May 2008, pp. 597-605.
- [18] N. Avazov, M. Patzold: 'A Geometric Street Scattering Channel Model for Car-to-Car Communication Systems', IEEE International Conf. on Advanced Technol. for Commun., Da Nang, Vietnam, 2-4 Aug. 2011, pp. 224-230.
- [19] G.R. MacCartney, J.H. Zhang, S. Nie: 'Path Loss Models for 5G Millimeter Wave Propagation Channels in Urban Microcells', IEEE Global Communications Conference (GLOBECOM), Atlanta, GA, 9-13 Dec. 2013, pp. 3948-3953.
- [20] C.X. Wang, X. Cheng, D.I. Laurenson: 'Vehicle-to-Vehicle Channel Modeling and Measurements: Recent Advances and Future Challenges', IEEE Commun. Magazine, vol. 47, no. 11, pp. 96-103, November 2009.
- [21] X. Cheng, C.X. Wang, B. Ai: 'Envelope Level Crossing Rate and Average Fade Duration of Nonisotropic Vehicle-to-Vehicle Ricean Fading Channels', IEEE Trans. on Intelligent Transportation Systems, vol. 15, no. 1, pp. 62-72, Aug. 2013.
- [22] M.E. Rasekh, F. Farzaneh, A.A. Shishegar: 'A Street Canyon Approximation Model for the 60 GHz Propagation Channel in an Urban Environment with Rough Surfaces', International Symposium on Telecommun. (IST), Tehran, Iran, 4-6 Dec. 2010, pp.132-137.
- [23] X. Cheng, C. X. Wang, D. I. Laurenson, S. Salous, and A. V. Vasilakos: 'An Adaptive Geometry-Based Stochastic Model for Non-Isotropic MIMO Mobile-to-Mobile Channels', IEEE Trans. Wireless Commun., vol. 8, no. 9, pp. 4824-4835, Sept. 2009.
- [24] S.B. Wu, C.X. Wang, E.-H.M. Aggoune: 'A Non-Stationary 3-D Wideband Twin-Cluster Model for 5G Massive MIMO Channels', IEEE Journal on Selected Areas in Commun., vol. 32, no. 6, pp. 1207-1218, 2014.
- [25] Y. Yuan, C.X. Wang, X. Cheng: 'Novel 3D Geometry-Based Stochastic Models for Non-Isotropic MIMO Vehicle-to-Vehicle Channels', IEEE Trans. on Veh. Technol., vol. 13, no. 1, pp. 298-309, Jan. 2014.
- [26] X. Cheng, C.X. Wang, D.I. Laurenson: 'An Adaptive Geometry-Based Stochastic Model for Non-Isotropic MIMO Mobile-to-Mobile Channels', IEEE Trans. on Wireless Commun., vol. 8, no. 9, pp. 4824-4835, Sep. 2009.



less communications.

**Hao Jiang** received his B.S. (2012), and M.S. (2015) degrees all from School of Electronics and Information Engineering, Nanjing University of Information Science and Technology, Nanjing, China. He is now pursuing Ph.D. degree in the National Mobile Communications Research Laboratory, Southeast University, Nanjing, China. His current research interests include wireless channel models and simulation, channel estimation and equalization, massive multiple-input and multiple-output wireless communication systems, and fifth-generation wire-



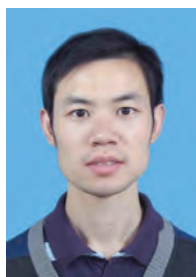
China in 2004 and is currently a Professor there. He has published over 150 papers and issued 20 patents. His current research interests include 5G wireless systems, optical wireless communication technologies, and quantum communications.

**Zaichen Zhang (M02-S15)** was born in Nanjing, China in 1975. He received BS and MS degrees in Electrical and Information Engineering from Southeast University, Nanjing, China in 1996 and 1999, respectively, and Ph.D. degree in Electrical and Electronic Engineering from The University of Hong Kong, Hong Kong, China in 2002. From 2002 to 2004, he was a Postdoctoral Fellow at the National Mobile Communications Research Lab., Southeast University, China. He joined School of Information Science and Engineering, Southeast University,



modulation schemes and visible light communications.

**Jian Dang** received the B.S. (2007) and Ph.D. (2013) degrees from the School of Information Science and Engineering, Southeast University, Nanjing, China. He is currently a Lecturer with the National Mobile Communications Research Laboratory, Southeast University. From September 2010 to March 2012, he was with the Department of Electrical and Computer Engineering, University of Florida, as a Visiting Student. His research interests include signal processing in wireless communications, multiple access schemes, non-orthogonal



communications, multiple input and multiple output wireless communication systems, and orthogonal frequency-division multiplexing.

**Liang Wu** received his B.S. (2007), M.S. (2010) and Ph.D. (2013) degrees all from School of Information Science and Engineering, Southeast University, Nanjing, China. From Sept. 2011 to Mar. 2013, he was with the School of Electrical Engineering and Computer Science, Oregon State University, as a visiting student. He is now a Lecturer with the National Mobile Communications Research Laboratory, Southeast University, Nanjing, China. His research interests include ultra-wideband wireless communication system, indoor optical wireless communications, multiple input and multiple output wireless communication systems, and orthogonal frequency-division multiplexing.